Analysis and Optimization of Nonlinear Diode Grids for Shielding of Enclosures With Apertures

Analysis and Optimization of Nonlinear Diode Grids for Shielding of Enclosures with Apertures

Cheng Yang, *Member, IEEE,* Torben Wendt, *Student Member, IEEE,* Marco De Stefano, *Student Member, IEEE,* Marc Kopf, Christopher Marc Becker, Stefano Grivet-Talocia, *Fellow, IEEE,* and Christian Schuster, *Senior Member, IEEE*

***Abstract*—Lumped-element grids provide an attractive option for wave propagation control in electromagnetic compatibility (EMC) engineering. This paper investigates the peak shielding effectiveness (SE) of a diode grid used for protection of enclosures with apertures against high intensity radiation fields (HIRFs). The nonlinearly loaded aperture is investigated with an efficient hybrid field-circuit simulation approach. Numerical experiments show that design aspects, e.g., aperture and enclosure size, grid density, impedance characteristic of lumped loads, play an important role in the field transmission through a diode grid which is nonlinear and time-variant. With a physics-based analysis of the interaction between the grid and the enclosure-backed aperture, nonlinear shielding techniques are identified that allow a control of the peak SE between 0 dB and 26 dB in novel ways. For the first time, the peak SE curve of a diode grid is demonstrated with four different field intensity dependencies, i.e., intensity low-pass, intensity high-pass, intensity band-pass and intensity band-stop selectivities from tens V/m to hundreds of V/m. By considering design aspects into a two-step optimization procedure, practical guidelines are provided for the nonlinear shielding implementation.**

***Index Terms*—Nonlinear shielding, diode grids, band-pass, band-stop, field intensity selectivity, hybrid simulation, guideline.**

I. Introduction

MODERN electronic systems with high speed signal processing and high frequency wireless communication suffer from susceptibility to high intensity radiation fields (HIRFs) or electromagnetic interferences (EMI) in general [1]. These interferences, rising from external electromagnetic (EM) radiation sources, such as electrostatic discharge, broadcasting transmitters, automotive radars, base stations, WIFI hotspots, IoT (Internet of Things) and 5G devices, can result in software failures or even hardware damages. For protection, various devices or materials can be used in system in order to shield, filter, limit or absorb intense radiation energy. Among them, nonlinearly loaded structures using lumped element arrays or grids have been receiving increasing attention and become an emerging research area in electromagnetic compatibility (EMC). For example, limiting frequency selective surfaces [2], [3], energy selective surfaces [4]–[6], waveform-dependent metasurfaces [7]–[9], power-dependent metasurfaces [10]–[13] and other nonlinear loaded designs [14]–[21]. On the experimental side, a large number of nonlinear design prototypes have been reported as depicted in Fig. 1, showing successful controls of nonlinear elements by strong radiation fields [3]–[7], [10], [12], [15], [18]–[20], [22]–[24], [24]–[27]. The nonlinearly loaded structures found applications in an intelligent, all-passive and self-configurable EMI protection for a single antenna or antenna arrays [19], [20], requiring no external sensors or biasing circuits.

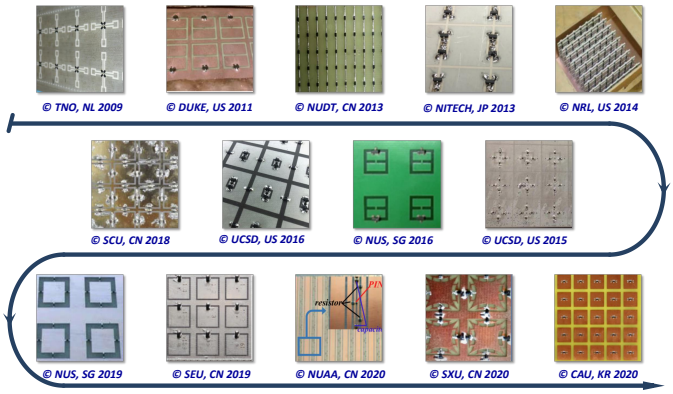

Fig. 1. Selected examples of nonlinear loaded structure designs using diode grids from [3], [4], [7], [10], [12], [15], [18]–[20], [22]–[26]. The number of utilized diodes is varying from 8 to 4050. All listed designs are self-activated and are published with high-power microwave experiments.

For illustration, Fig. 2 depicts an example of a nonlinearly loaded aperture with an aggressor and a victim positioned in front and center of the enclosure. The switching of the diodes affects the field penetration through the grid, making the high field intensity and low field intensity waves distinguishable, an effect that is labeled as nonlinear shielding in this paper. This offers the advantage of self-actuated and field intensity dependent characteristics of a diode grid, which allows a victim behind the diode grid to transmit/receive signals at low field intensity levels. However, the field transmission through a diode grid is also influenced by the resonances of the enclosure, making the implementation of nonlinear shielding difficult. Previous nonlinear loaded designs are either highly dependent on a computational expensive full-wave simulation or approximated with a simplified full-wave simulation using only one unit cell [3], [19], [24], [26], resulting in an inefficient iterative optimization [13]. To our best knowledge, there is

This work is supported in part by the German Research Foundation (DFG).

C. Yang, T. Wendt and C. Schuster are with the Institut für Theoretische Elektrotechnik, Technischen Universität Hamburg, D-21073, Hamburg, Germany (e-mail: cheng.yang; torben.wendt; schuster@tuhh.de).

M. De Stefano and S. Grivet-Talocia are with the Department of Electronics and Telecommunications, Politecnico di Torino 10129, Torino, Italy (e-mail: marco.destefano; stefano.grivet@polito.it).

Manuscript received 15 Nov., 2020; revised 24 Feb., 2021.

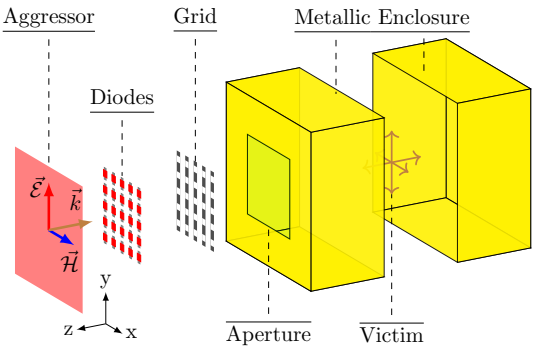

Fig. 2. Depiction of a diode grid used for shielding of an aperture backed with a metallic enclosure. An aggressor and a victim are positioned in exterior and interior region of the enclosure. Nonlinear shielding is accomplished with the switching of the diodes by an incident field.

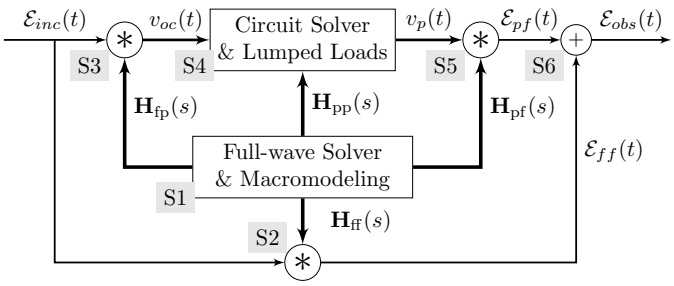

Fig. 3. Flowchart of a hybrid field-circuit simulation, performed in six steps (S1-S6) for computation of circuit and field responses in time and frequency domain. The hybrid approach offers the advantage that changing lumped loads has no impact on S1-S3, leading to an efficient and fast simulation.

no closed-form solution and very few guidelines have been reported for an optimized design of a diode grid for enclosures. Therefore, the emphasis in this work is put on the design optimization of a nonlinear shielding design using an efficient hybrid field-circuit simulation approach [28], as well as exploiting new possibilities of nonlinear shielding. Specifically, important design aspects, such as enclosure and aperture size, grid and diode parameters, have been studied by extensive parameter sweeps. The nonlinear shielding effectiveness (SE) of a diode grid will be explained in detail with physical insights; the design of nonlinear SE has been developed with an efficient and flexible optimization procedure, and the field intensity dependent characteristic of a diode grid has been extended with more interesting features. The physical size of all lumped elements are assumed to be electrically small and the modeling of such elements is implemented as a general circuit netlist at the loading point.

The remaining of this paper is organized as follows. In Section II, the simulation approach is briefly introduced and a nonlinear SE curve is taken for studying nonlinear shielding effects with physical understanding. Using geometry and circuit parameter sweeps, the optimization of nonlinear shielding is discussed in Section III, showing flexible manipulations of nonlinear SE curves. Section IV summarises practical design strategies and provides guidelines for nonlinear shielding design. Conclusions are given in Section V.

II. Analysis of Nonlinear Shielding

Shielding of enclosures using linear elements, such as wires, screens, apertures, etc., is well understood and well documented in literature [29]–[32]. In contrast, closed-form solutions to nonlinear shielding problems are beyond reach and a numerical simulation has to be undertaken. For analysis of enclosures loaded with massive nonlinear elements, an efficient hybrid simulation approach is described in the following.

A. Hybrid Field-Circuit Simulation Approach

To solve the problems of this study, a hybrid field-circuit simulation based on frequency domain data is utilized. Originated in the 1970s for solving wire antenna problems [33], this approach saw increased interests over the last decades [28], [34]–[37]. Its advantages are that impulse responses of the structure, characterized as a linear time-invariant (LTI) system, can be repeatedly used for transient simulations, saving computational effort. Interim results can be recycled for parameter sweeps, which is not possible by choosing transient full-wave field-circuit simulations [38]–[40].

Fig. 3 outlines the flow of the simulation approach. The incoming wave excitation $\mathcal{E}_{inc}(t)$ is taken as an input for computation of the received field $\mathcal{E}_{obs}(t)$ as an output in six steps (S1-S6). Based on generalized Thevenin's theorem and the superposition theorem, $\mathcal{E}_{obs}(t)$ is decomposed into two portions, i.e. $\mathcal{E}_{pf}(t)$ and $\mathcal{E}_{ff}(t)$, in dependence (upper branch) and independent (lower branch) of the lumped loads. Here, f or p are abbreviations of fields or ports, respectively, where a port is defined at the loading point of lumped elements attached to the structure, as popularly used in wire antenna problems for loading lumped elements at terminals [33]. Following the upper (S3-S5) and the lower (S2) branches, several transfer functions are considered successively, including $\mathbf{H}_{\mathrm{fp}}(s)$, $\mathbf{H}_{\mathrm{pp}}(s)$, $\mathbf{H}_{\mathrm{pf}}(s)$ and $\mathbf{H}_{\mathrm{ff}}(s)$, which stand for macromodels of field-port, port-port, port-field and field-field responses in frequency domain, such as open-circuit (OC) voltages, admittance parameters and field responses. Simultaneously, intermediate results, such as $\boldsymbol{v}_p(t)$ and $\boldsymbol{v}_{oc}(t)$, port voltages with and without lumped elements, are calculated. More details of the approach, including step by step derivation and numerical complexity explanation, can be found in publications [28], [37], [41]. The framework was implemented in a general purpose computation environment [42] and combined with a method of moment (MoM) based in-house full-wave simulator [43] and a commercial circuit simulator [44]. Concerning the macromodeling via vector fitting [45], [46], all fields related frequency transfer functions are processed in the computation environment [42] and the port to port transfer functions, i.e. network parameters, are translated to a circuit netlist using a commercial software [47] with passivity enforcement. Specifically, when all port loadings are linear, the simulation can be accelerated by replacing S2-S6 with linear analysis in frequency domain and S6 with a fast recursive convolution. For validation, an enclosure-backed aperture loaded with a 3×3 resistor grid is adapted, detailed modeling and simulation from [37]. Simulation results

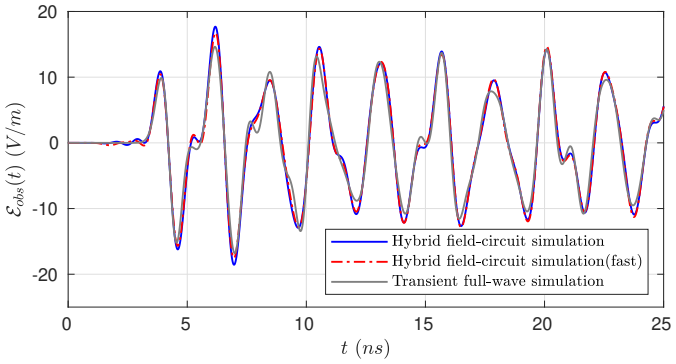

Fig. 4. Comparison of transient penetrating fields through a 3×3 50Ω resistor grid obtained by various simulation approaches. The transient full-wave simulation is provided by a commercial software [47].

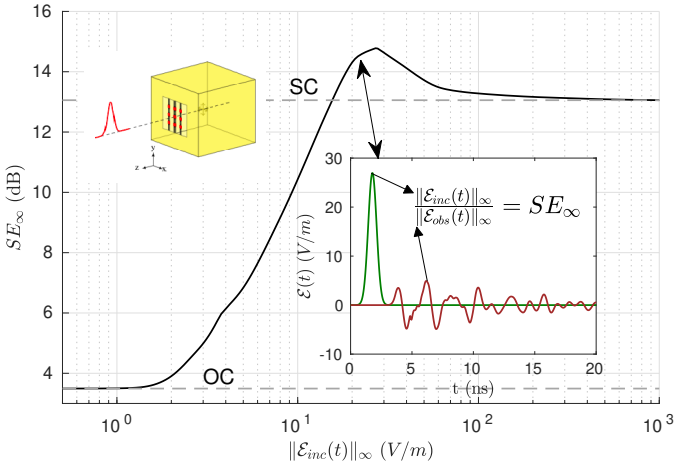

Fig. 5. Nonlinear SE curve of a 3×3 diode grid loaded aperture obtained by an intensity sweep of the incident waves. Transient receiving fields are observed at the center of the enclosure. An example is shown as inset with comparison to the incident field.

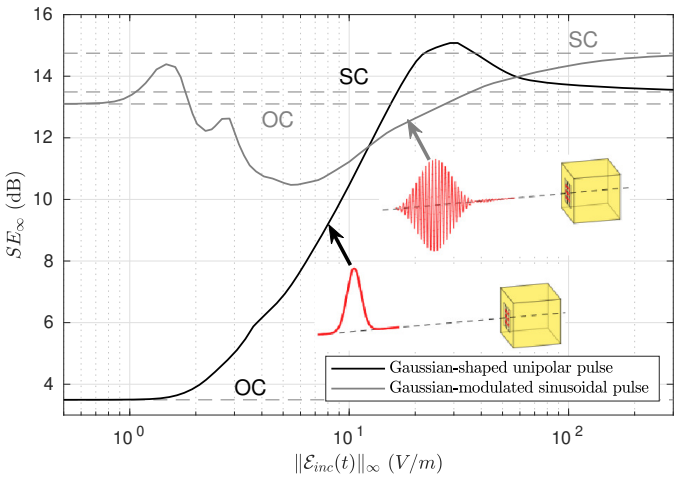

Fig. 6. Comparison of nonlinear SE curves of a 3×3 diode grid loaded aperture with respect to incident signals of different signature in time and relative bandwidth.

are shown in Fig. 4 with a good agreement. Based on a Intel Core i7-4930K Processor with 6 CPU cores running at 3.4 GHz, a repetitive transient full-wave simulation with a 1/50 wavelength discretization of the passive structure needs about 15.5 hours for the computation of $\mathcal{E}_{obs}(t)$ of 40 ns length, while a repetitive hybrid field-circuit simulation takes less than 5 seconds, showing the advantage of recycling impulse responses provided by generated macromodels in step S1. It should be pointed out that, the computation time in S1, i.e. creating macromodels from full-wave simulations, is excluded for repetitive simulations.

B. Definition of Nonlinear Shielding Effectiveness

Considering the maximum intensity of penetrating electric fields as the main threat from external EMI, a peak SE defined in time domain is calculated as

$$SE_\infty(\vec{\mathbf{r}}) = \frac{\|\mathcal{E}_{inc}(t)\|_\infty}{\left\|\vec{\mathcal{E}}_{obs}(t,\vec{\mathbf{r}})\right\|_\infty} \tag{1}$$

where $\mathcal{E}_{inc}(t)$ stands for the incident E-field, $\vec{\mathcal{E}}_{obs}(t,\vec{\mathbf{r}})$ for the received E-field at an observation point $\vec{\mathbf{r}}$. The operator $\|\cdot\|_\infty$ extracts the largest magnitude of its vector augment over time. The thus defined nonlinear SE is depending on the amplitude and signature of the incident wave, the diode grid, the aperture and the position in the enclosure where the field is received. Due to the diodes, the SE curve shows a field intensity dependent behavior, i.e. nonlinear shielding.

In general, nonlinear shielding can be categorized by establishing two cases, an OC grid and a short-circuit (SC) grid, that bound the nonlinear behavior at extremely low and high field intensity levels. An OC or SC grid is obtained by enforcing all diodes turned OFF or ON at ports, or equivalently by loading each port with zero conductance or zero resistance. For illustration, Fig. 5 presents a nonlinear shielding curve of a 3×3 diode grid loaded aperture backed with a metallic cavity. Each column of the diode grid consists of 3 pairs of anti-parallel PN junction diodes and 4 pieces of metal strips with the top and the bottom ones connected to the metallic cavity [37]. As seen, the two ends of the curve approach two asymptotes with SE value of 3.5 dB and 13.5 dB. Considering the fact that a lower peak SE corresponds to a higher field penetration, the SE curve of Fig. 5 is classified as an "intensity low-pass" type nonlinear shielding. Later in this paper, it will be shown that more types of SE curves can be obtained by efficient numerical optimizations of selected design aspects.

C. Shielding Performance of OC and SC Grids

For an enclosure-backed aperture shielding, it is assumed that an OC grid allows more field penetration than an SC grid. However, this assumption may be violated by many factors, such as the spectrum of an incident wave, the geometry size of a background structure and an aperture, the density of a grid, and the location of a victim. For demonstration, the 3×3 diode grid example, used in Fig. 5, is revisited with a short-time Gaussian pulse wave excitation replaced by a narrow-band wave excitation. Simulation results are shown in Fig. 6. The nonlinear shielding performance of the same diode grid is degraded by less than 3.0 dB SE deviation between OC and SC limits. Further simulations show that an SC grid shows

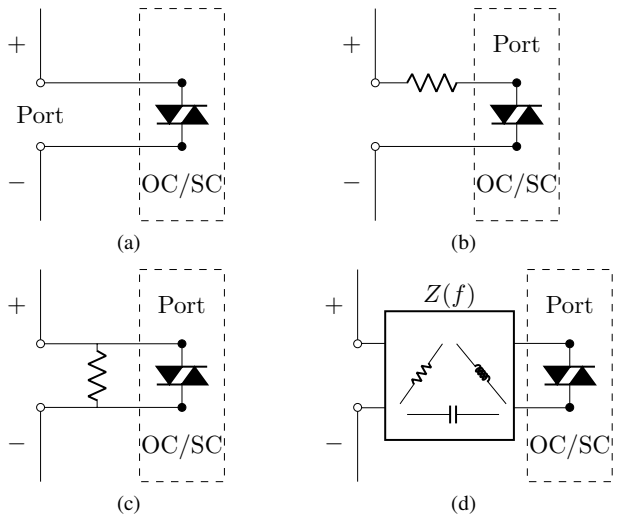

Fig. 7. Illustration of linear loading at each port of a diode grid: (a) an original port and three modifications by inserting (b) a series resistor, (c) a parallel resistor, and (d) a cascaded two port linear network with the original port which affects the OC and SC limits of a diode grid.

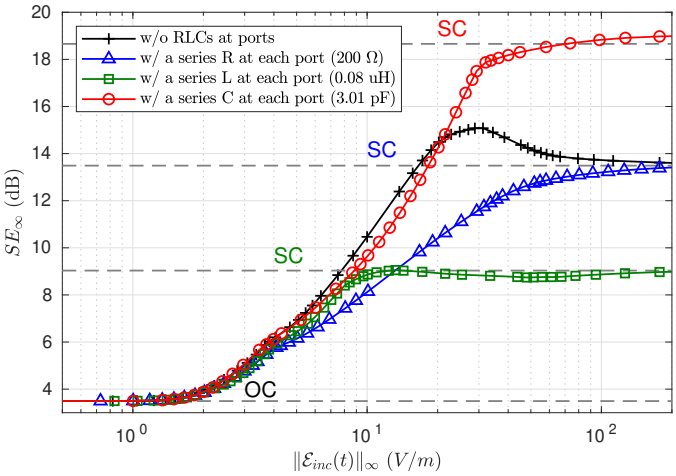

Fig. 8. Comparison of nonlinear SE curves provided by a modified 3×3 diode grid loaded aperture with different loading at ports. As can been seen, only the ON state of a diode grid is influenced.

an even worse shielding performance than an OC grid, in the case that the center frequency of the incident wave coincides with the resonances of the enclosure.

Another way of changing OC and SC limits of a nonlinear SE curve is to vary loadings at ports. Fig. 7 lists several variations of OC and SC grids by loading additional linear lumped-elements at ports. As can be seen, the SC grid defined by Fig. 7(b) is identical to the OC grid provided by Fig. 7(c). Therefore an OC or SC classification of a grid is not sufficient unless the port definition is specified. Taking Fig. 7(b) for demonstration, an SC grid is modified with a resistor (R), an inductor (L) or a capacitor (C) in series with the original port, respectively. By tuning the value of R, L, and C, the field penetration through a newly defined SC grid can be customized. Possible peak SE values of the new SC grid are obtained by parameter sweeps using fast hybrid field-circuit simulations. It is found that using either a series R or C at

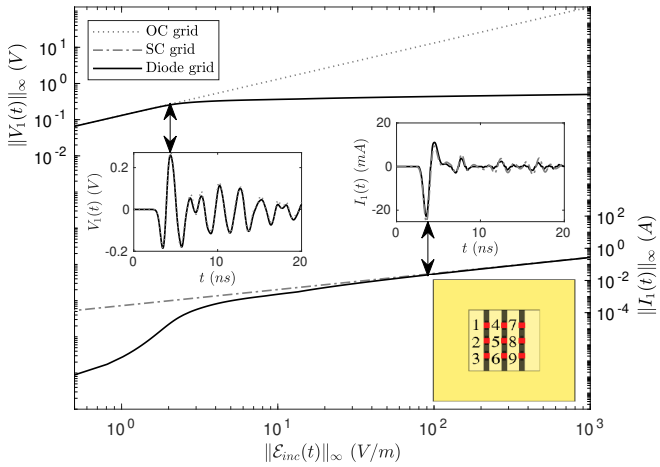

Fig. 9. Voltage and current responses at port 1 of a 3×3 diode grid loaded aperture, with comparison to an OC grid and an SC grid. The maximum magnitude of port responses is extracted with respect to incident waves with different field intensities.

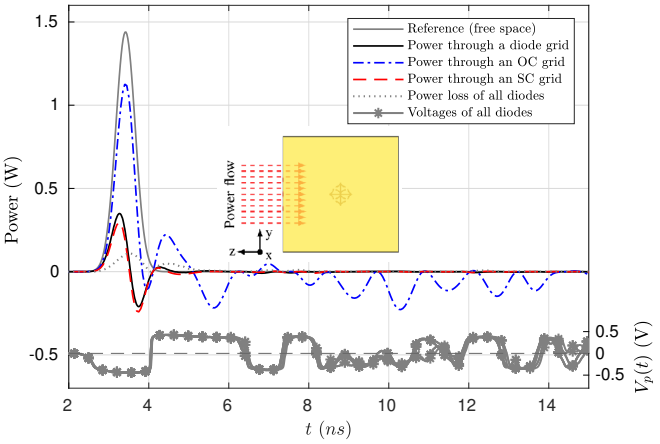

Fig. 10. Comparison of power through an enclosure-backed aperture with different grids, including a 3×3 diode grid, an OC grid and an SC grid, at a high field intensity level, $\|\mathcal{E}_{inc}(t)\|_\infty$ = 100 V/m. The power loss of the diodes is given for relevance.

each port can achieve a higher peak SE. This is verified by conducting nonlinear shielding investigations with simulation results shown in Fig. 8. As seen, the peak SE values of a modified diode grid can be flexibly tuned at higher field intensity levels. Similarly, the OC limit can be modified by adding parallel RLCs at ports without changing the SC limit.

Based on the above analysis, it is clear that a diode grid can be approximated by considering OC and SC grids at extremely low and high field intensity levels. It is also clear that the OC and SC limits of a diode grid can be tuned by modifying port loading. For more general modification of OC and SC limits, the geometry size of the background structures and the grid can be optimized which will be discussed in Section III.

D. Power Loss of a Diode Grid

Due to the switching of the diodes, the shielding performance of a diode grid loaded aperture is varying in a range that is generally bounded by OC and SC limits. In order to understand how the diodes are influenced by incident

fields, voltage and current responses, taken from port 1 of a 3×3 diode grid, are observed with results shown in Fig. 9. Comparing to the responses of OC and SC grids, the voltage at port 1 is limited under the threshold voltage of diodes, about 0.5 V; the current at port 1 is approaching the SC current at high field intensity levels. It should be pointed out that the ON-state of diodes at port 1 is not sustained if the port voltage drops below the threshold value. Consequently, the diodes at port 1 would be switched ON and OFF multiple times, which is the same for other ports.

However, the switching of a diode grid results in not only a time-variant reflection of the grid, but also an Ohmic loss of power. Due to the dynamic resistance of diodes during the switching, the SE value of a diode grid can even exceed OC and SC limits which can be explained from the point of view of power loss. By comparing the power through a nonlinear loaded aperture under a strong intensity field radiation, $\|\mathcal{E}_{inc}(t)\|_{\infty}$ = 100 V/m, the nonlinear behavior of a diode grid is studied in Fig. 10. As seen, the ON-state of the diode grid, indicated by port voltages with the threshold value, dominates during the first 8 ns. Therefore, the power through a diode grid is dramatically decreased by reflections, as well as the power loss of the diodes, giving a considerable field attenuation as shown in Fig. 5. Besides, if the incident field intensity becomes extremely high, the diodes switch to ON state and the Ohmic loss of all diodes is negligible when comparing to the incident and reflected power. In such a circumstance, a diode grid behaves as an SC grid.

To sum up, nonlinear shielding of a diode grid is realized as a field intensity dependent control of electromagnetic field energy in a space. The control is based on a time-variant adjustment of the coupling between the linear and the nonlinear parts of the structure, resulting in a real-time changing of reflection loss, wave absorption and field penetration. For the practice of a nonlinear shielding, various design aspects, such as geometry parameters of the grids, the aperture and enclosure, circuit characteristics of the lumped elements, setup configurations of a wave excitation and field observations, should be considered.

III. Optimization of Nonlinear Shielding

A nonlinear shielding design can be either implemented as a separated component to the device, such an antenna radome [13], or integrated into the device or system, such as a metallic enclosure with openings. Without loss of generality, we continue using the example of a diode grid loaded aperture and a short-time Gaussian pulse wave excitation for demonstration and optimization. Unless otherwise specified, the default size of the enclosure, the aperture and the dimension of the lumped element array are 50×50×50 cm^3, 25×25 cm^2 and 8×8. To reduce the design complexity, the main features of nonlinear shielding, i.e. the minimum, the maximum and the transition of a nonlinear SE curve, are taken as the goal of optimization. By conducting subsequent linear and nonlinear analysis of the selected structure and circuit parameters, a two-step optimization procedure is proposed here as given by Fig. 11. First, considering the asymptotes of the nonlinear SE

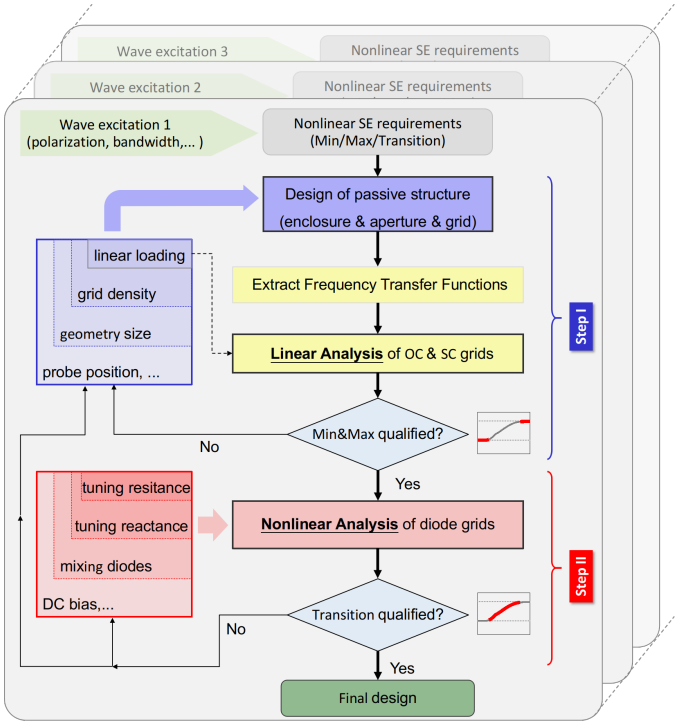

Fig. 11. A two-step optimization procedure for nonlinear shielding practice. Each profile contains an optimization of different features of a nonlinear SE curve with respect to a wave excitation.

curve as an optimization goal, linear analysis is utilized for tuning the OC and SC limits of a diode grid. Based on a large number of numerical simulations of enclosure-grid examples, three main design aspects, i.e. the size of the structure, the grid density and linear loading at ports, have been identified for optimization of the shielding of a short-time Gaussian pulse planar wave excitation. Second, the transition of a SE curve is optimized by conducting nonlinear analysis of a diode grid. Consequently, the nonlinear SE curve can be flexibly adjusted by changing or exchanging lumped-element loading at ports. Besides, special attention should be paid on the spectrum feature of an incident wave which significantly affects the OC and SC limits of a diode grid. For example, according to Fig. 12b, the field transmission through an OC and an SC grid doesn't differ much at about 600 MHz for the particular structure used for illustration. As a result, a nonlinear peak SE curve corresponding to a narrow-band wave excitation with a center frequency of 600 MHz is often not appropriate for use, as shown in Fig. 6. In such a case, the field transmission coefficient should be changed either by modifying the structure or adding RLCs at ports.

A. Changing Structure Size and Grid Density

In order to obtain sufficient changes between OC and SC limits, the field transmission through OC and SC grids is first optimized in frequency domain, towards an acceptable deviation within the frequency range of interest, 15.0 dB for example. Four selected enclosure-backed apertures are investigated with the same grid density of 2.78×2.78 cm^2 per unit cell. Fig. 12 shows the simulated frequency responses of

OC and SC grids for each aperture. From Fig. 12a to Fig. 12c, the side length of the enclosure is fixed at 50 cm. Simulation results show the magnitude of the frequency responses is proportional to the size of the aperture, which is varying from 13.9×13.9 cm^2 to 36.1×36.1 cm^2. Simultaneously, the sharp resonant peak at around 420 MHz is eliminated due to larger openings of the aperture. Based on the setup in Fig. 12b, the side length of the enclosure is extended up to 75 cm. As the enclosure size increases, the fundamental resonant frequency of the passive structure is decreased from 420 MHz to about 260 MHz. Consequently more and more resonance peaks move into the frequency range below 750 MHz, as seen in Fig. 12d. Then the nonlinear SE curve is verified in time domain as shown Fig. 13. Based on the four cases, it is found that an increase of the relative size of the aperture to enclosure shifts the curve up and to the left, whereas the distance changing between two asymptotes is negligible because the grid density remains the same. Once the geometry size of the aperture and the enclosure is fixed, changing of grid density plays an important role in adjusting the peak SE of SC grids. For illustration, Fig. 14 presents the frequency response of a SC grid with scale varying from 3×3 to 15×15. As expected, the field penetration can be effectively reduced by increasing the grid density, except for a few resonance frequencies. Based on nonlinear SE curves shown in Fig. 15, only the upper asymptote is shifted because the lower asymptote is dependent on the field transmission of OC grids. It is also observed that the transition part of the nonlinear SE curve is influenced because a larger number of diodes along each column of grids require higher field intensity to switch.

B. Adding Linear RLCs at Ports

In addition of changing geometry parameters, an alternative way to optimize the asymptotes of nonlinear SE curves is to use linear loads at ports. It has been shown that any linear lumped element grids can be defined as OC or SC grids by properly relocating the port position, see Fig. 7. In principle, a linear loading at a port could be an arbitrary circuit, the choice being limited by the physical size of the elements and the space around a port. Here, each linear load at the port is considered a two-element RLC combination with a connection either in series or in parallel with each other. By applying identical linear loadings at all ports, an optimization of RLC values is first attempted by direct parameter search in a range with 100 discrete samplings, leading to 10k simulations for each linear grid. The peak SE values with respect to a wide-band wave excitation are shown in Fig. 16. Apparently, RLC combinations provide a good ability for controlling field transmission through the aperture. Especially, when the peak SE value varies between 4.0 dB and 14.0 dB, LC grids show dramatic variations in the center (L = 1.0 uH and C = 1.0 pF), indicating strong couplings in this region.

In order to go beyond the asymptotes bounded by the original OC and SC grids, another 800 simulations are added to find optimized RLC values with an adaptive searching approach. All simulated peak SE values are shown in Fig. 17. By comparing the maximum and the minimum of each curve, a grid with C elements loading at ports exceeds the limits of both OC and SC grids. Specifically, the increase of field penetration is not observed by using a single RLC element in previous investigations of a 3×3 grid. It should be pointed out that the optimized RLC values may be different from excitation to excitation. Because the changing of the active frequency band affects the coupling between grids and enclosure-backed aperture.

The modification of asymptotes causes an inevitable influence on transitions between OFF- and ON-states of a diode grid. In order to compensate undesired nonlinear transitions, consisting of numerous intermediate states, the nonlinearity of the grid is tuned by changing the circuit parameters of the diodes. In the following, we will show the feasibility of shifting, flipping, and mixing nonlinear transitions by only playing with diodes.

C. Tuning Nonlinear Elements

The first circuit parameter of diodes in consideration is the threshold voltage, which is mainly determined by the semiconductor materials. For PN junction diodes, the voltage to current (V-I) characteristic is described as

$$i(t) = I_s \cdot \exp\left[\frac{v(t)}{nV_T}\right] - I_s \tag{2}$$

where $i(t)$ and $v(t)$ correspond to the diode current and voltage, I_s is the reverse saturation current, n is the ideality factor and V_T is the thermal voltage, specified as 26 mV at room temperature [37]. Table I lists the modeling parameters of diodes used in previous simulations, together with Gallium Arsenide (GaAs), Silicon (Si) and Germanium (Ge) diodes for comparison.

TABLE I
MODELING PARAMETERS OF PN JUNCTION DIODES USED IN TRANSIENT SIMULATIONS [48]

Diode type	Saturation current	Ideality factor
Default (This)	1 nA	1.00
Gallium Arsenide (GaAs)	1 pA	2.00
Silicon (Si)	10 pA	1.00
Germanium (Ge)	1 uA	0.67

The peak SE curves of different diode grids are shown in Fig. 18 and the V-I curves are given as inset. The threshold voltages of four different diodes are about 0.25 V, 0.50 V, 0.70 V and 1.30 V respectively. The higher the threshold voltage is, the stronger the incident fields have to be for switching of a diode grid. Therefore, changing the threshold voltage of diodes is an effective way to shift nonlinear SE curves with respect to field intensity. For example, Schottky and Zener diodes, with different threshold voltages, e.g. 150 mV or 10.0 V, can be employed.

In addition of tuning the resistance of a diode adjusting the reactance of a diode provides another opportunity for

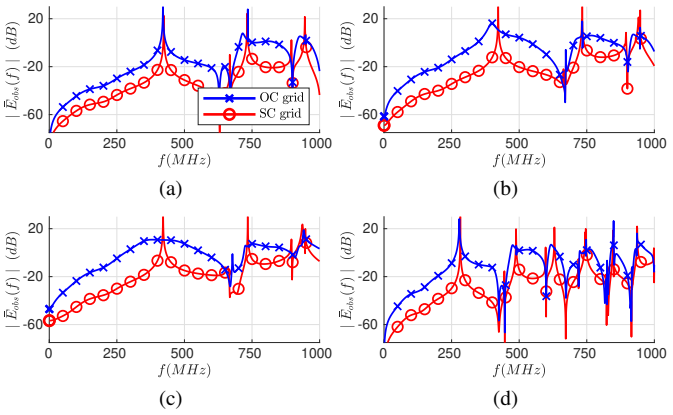

Fig. 12. Comparison of normalized field transmission coefficients for different aperture sizes (a) 13.9×13.9cm^2, (b) 25.0×25.0 cm^2, (c) 36.1×36.1 cm^2 and a different enclosure size (d) 75×75×75 cm^3.

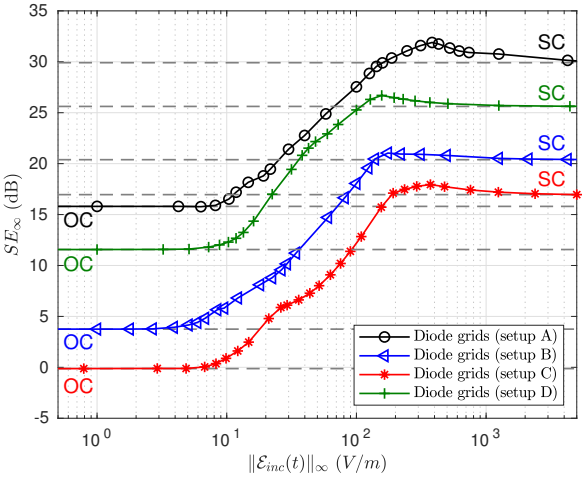

Fig. 13. Comparison of nonlinear SE curves of a 8×8 diode grid with respect to different size of aperture and enclosure. Setups A-D are corresponding to Fig. 12a-12d, respectively.

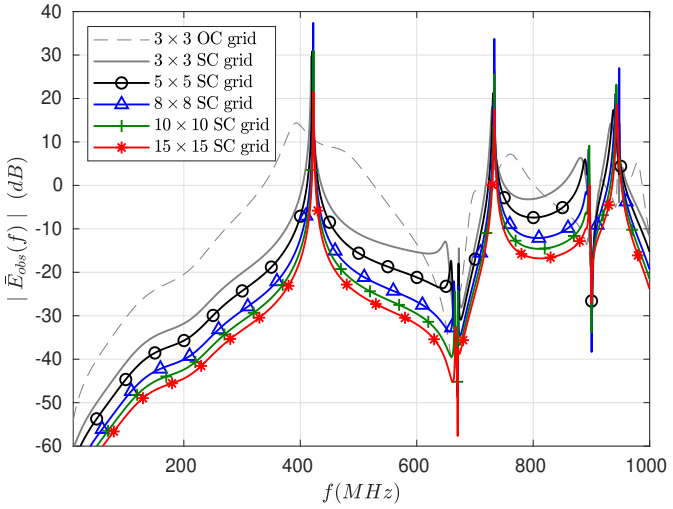

Fig. 14. Comparison of normalized field transmissions through OC or SC grids with different grid density.

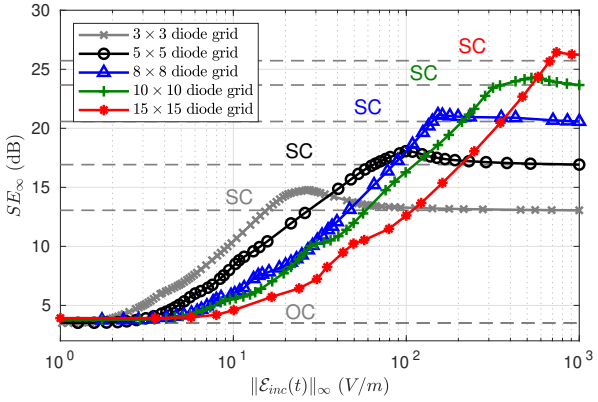

Fig. 15. Comparison of nonlinear SE curves of a 8×8 diode grid with different grid density.

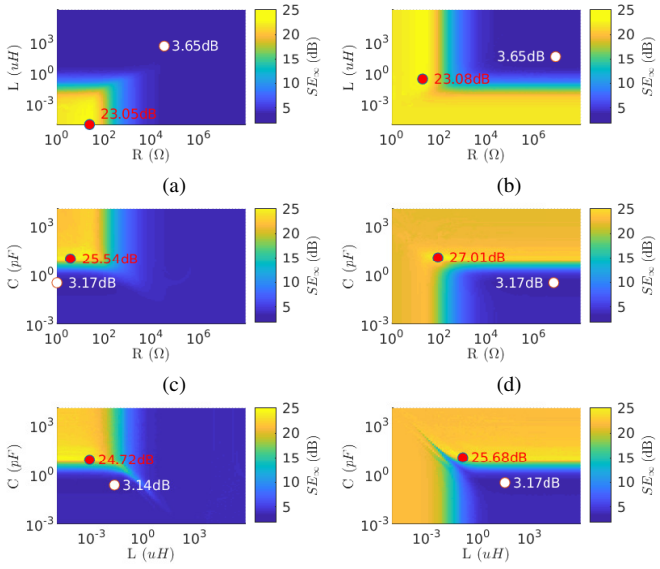

Fig. 16. Comparison of peak SE values for modified grids with different type of loading at ports: (a) R-L (b) R||L (c) R-C (d) R||C (e) L-C (f) L||C.

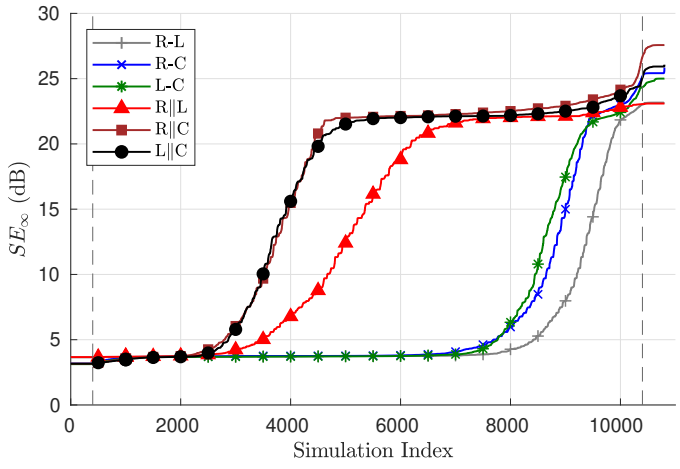

Fig. 17. Illustration of peak SE variations with linear loading at ports. Based on Fig. 16, all simulations are sorted by peak SE values such that an index is utilized for labeling different RLC loading in each case.

nonlinear shielding design. Varactor diodes, for example, show a junction capacitance that is reverse voltage dependent [49]

$$C_J(v_R(t)) = \frac{C_{J0}}{1 + \left(\frac{v_R(t)}{V_J}\right)^M} \tag{3}$$

where C_{J0} denotes the zeros-bias junction capacitance, $v_R(t)$ stands for the applied reverse voltage, V_J is the junction potential, and M is the grading coefficient. Since $C_J(v_R(t))$ of a varactor diode is inversely proportional to $v_R(t)$, a pair of back to back varactor diodes performs an opposite switching at ports, i.e. SC to OC, resulting in a flipped peak SE curve. Furthermore, when properly tuning the resistance and the reactance of diodes, the peak SE curves can be modulated as band-pass or band-stop.

TABLE II
MODELING PARAMETERS USED IN SIMULATION OF DIODES WITH VARIOUS VOLTAGE DEPENDENT RESISTANCE OR REACTANCE

Diode type	Circuit parameters	Symbol
PN junction	I_s = 1nA, n = 1	
Zener	Is = 1nA, n = 1, BV = 25V, I_{bv} = 1mA, R_s = 0.1Ω	
Varactor 1	Is = 10pA, n = 1, M = 4, C_{JO} = 16.13pF, V_J = 8	
Varactor 2	Is = 10pA, n = 1, M = 4, C_{JO} = 16.13pF, V_J = 2	

BV and I_{bv}-reverse breakdown voltage and current, R_s-series resistance

For demonstration, four types of diodes, as listed in Table II, are utilized for realizing intensity low-pass, high-pass, band-stop and band-pass type of nonlinear shielding designs. Specifically, a pair of antiparallel PN diodes with a threshold voltage of 0.5 V and a pair of back to back Zener diodes with a threshold voltage of 25.5 V are used in Fig. 19a and Fig. 19b, respectively. A pair of back to back varactor diodes are employed in Fig. 19c and Fig. 19d. The peak SE curves in Fig. 19e and Fig. 19f are obtained by connecting corresponding pairs of diodes from Fig. 19a-Fig. 19d in series and in parallel with each other, respectively. Following this idea, the more number of nonlinear elements are loaded at the port, the more kinds of nonlinear SE curves can be designed.

D. Mixing Diodes in Grids

Inspired by coding metamaterials [50], another possible way to manipulate nonlinear shielding is to load different types of diodes at different ports, i.e. mixed nonlinear loading at a grid level. Considering two types of diodes with different threshold voltages, e.g. Ge and GaAs diodes, used for a 8×8 diode grid design, there will be in principle $2^{64} \approx 1.84 \times 10^{19}$ possible nonlinear shielding solutions. By marking antiparallel Ge and GaAs diodes as "0" and "1" in a grid, a "0-1" pattern is used for the description of the mixed loading of diodes in a grid. Fig. 20 presents the peak SE curves corresponding to five typical patterns, covering different symmetries in row and column directions in grids. As expected, the peak SE curves of Ge and GaAs diode grids set the border for all peak SE values. Whereas the remaining three show different features. Especially, when different types of diodes are positioned alternatively along the column direction, the grid pattern denoted as $\binom{01}{01}$, the nonlinear shielding shows multiple transitions between multiple steady states. Nonlinear shielding design utilizing a chessboard pattern, denoted as $\binom{10}{01}$, and a row alternative pattern, denoted as $\binom{00}{11}$, does not show any difference because the exchanging of different diodes along one column does not matter.

IV. DISCUSSION AND DESIGN GUIDELINES

In order to perform a nonlinear shielding design, it is important to know: (1) how many steady states of grids are required, and (2) how to choose and configure nonlinear elements for nonlinear switching. To answer these two questions, we first list all functional modifications of peak SE curves according to all previous investigations. As depicted in Fig. 21, four basic manipulations are summarized here with related examples and design hints:

1) **Shifting**. Move the OC and SC limits of a nonlinear SE curve horizontally or vertically without significant impacts on the transition part. Effective optimizations can be achieved by changing the enclosure and aperture size (Fig. 13), and adjusting threshold voltage of diodes (Fig. 18).
2) **Scaling**. Compress or stretch a peak SE curve either horizontally or vertically. This can be obtained by changing grid density (Fig. 15), adding single resistor (Fig. 8) or proper RLC combinations at ports (Fig. 16).
3) **Flipping**. Exchange the OC and SC limits of a peak SE curve and modifying the transition part accordingly. Typical measures include adding proper capacitance (Fig. 16) or using varactor diodes at ports (Fig. 19c, Fig. 19d).
4) **Combining**. Modify the OC/SC limits and the transition part of a peak SE curve by superpositing multiple curves. This function can be realized by connecting multiple type of diodes at ports (Fig. 19e, Fig. 19f) or mixing different type of diodes in grids(Fig. 20).

Following the four categories, a peak SE curve can be optimized through parameter sweepings of aforementioned design aspects in Sec. III. However, different modification of a peak SE curve requires different optimization efforts. For example, both the shifting and scaling manipulations can be achieved by modifying either the passive structure or the port loading, resulting in a big difference of computation time. Since any changing of the geometry, such as the size of an enclosure, an aperture and a grid, or the loading points of lumped elements, requires a new full-wave frequency simulation with proper frequency samplings, the computation time can be varying from seconds to hundreds of hours or even more, dependent on the selected frequency sampling scheme, the discretization of the passive structure and the number of lumped loads. For instance, a Y-parameter simulation of a cavity example with 900 ports and 2000 frequencies takes about 65 hours

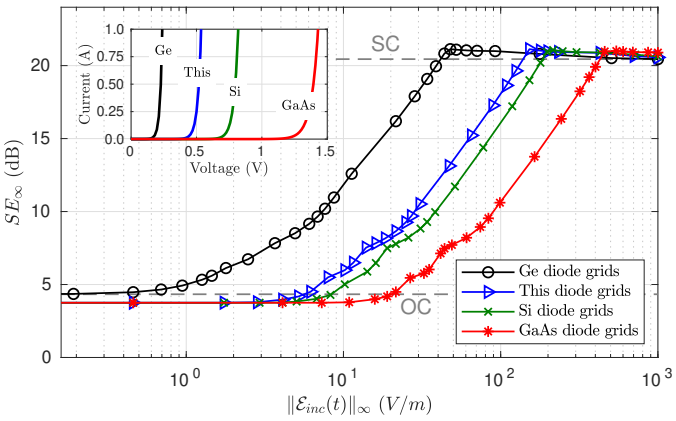

Fig. 18. Comparison of peak SE curves of a 8×8 diode grid loaded aperture with different threshold voltages as given in insets.

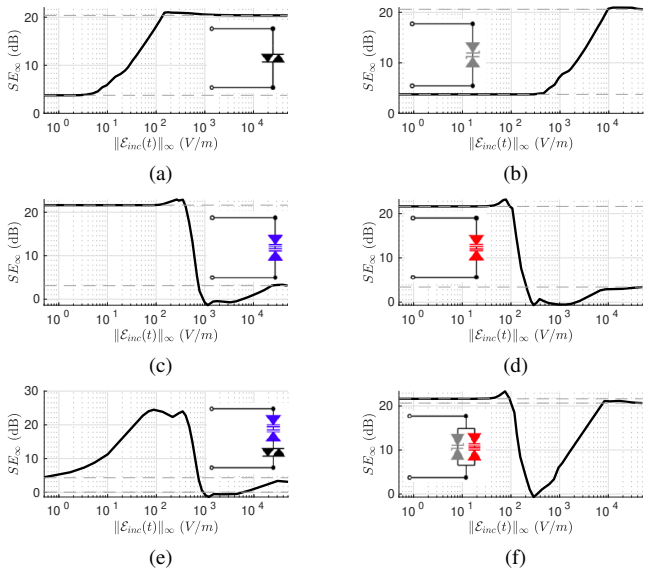

Fig. 19. Demonstration of field intensity selectivity of a 8×8 diode grid loaded aperture in different form of (a-b) intensity low-pass, (c-d) intensity high-pass, (e) intensity band-stop and (f) intensity band-pass. PN junction diodes, Zener diodes and varactor diodes and their combinations are utilized for design, as shown in insets.

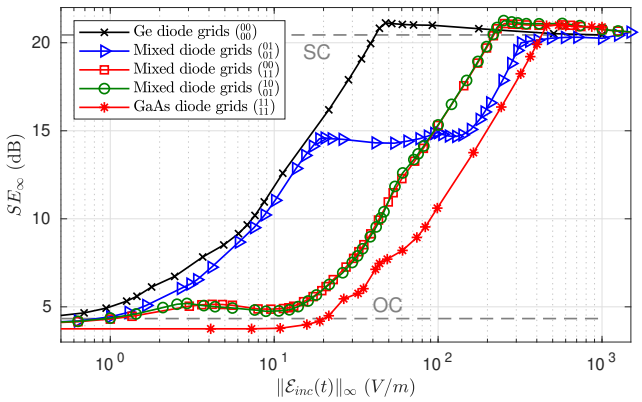

Fig. 20. Comparisons of peak SE curves of a 8×8 diode grid with mixed nonlinear loading in a grid. For each port, either Ge or GaAs diodes is loaded, which is denoted as "0" or "1" respectively.

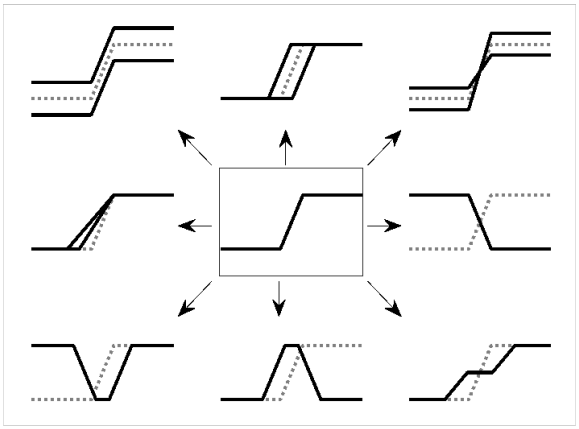

Fig. 21. Functional modification and extension of nonlinear shielding of a diode grid based on an intensity low-pass type SE curve.

using a 8 × 12 nodes cluster with 8 Intel Core i7-4930K Processors running at 3.4 GHz. By contrast, a pure hybrid field-circuit simulation with respect to the port loading is much more computational efficient and hence is recommended for the optimization whenever possible. Considering the other two manipulations, i.e. flipping and combining, the optimization is conducted by modifying loads at ports and therefore can be conducted efficiently. Besides, in order to speed up the parameter sweeps and to capture fine features of a SE curve as possible, for example, maximum/minimum values and sharp peaks, an adaptive parameter sampling scheme is recommended for all linear and nonlinear investigations.

With efficient parameter sweeps, a peak SE curve can be optimized with a two-step procedure as given in Fig. 11. Starting from an initial design, the field penetration through OC and SC grids is investigated in frequency domain. To find an interesting range of geometry parameters, a transmission line based analytical method, with a good approximation accuracy up to GHz, can be used for reducing the computation efforts of full-wave optimization [31], [32], [51]–[53]. Then a linear analysis is conducted by taking a specified incident wave excitation into account. OC and SC limits and other possible steady states, if existing, are estimated. If any of the steady states is not satisfactory, the design will be optimized by shifting or scaling the asymptotes vertically, i.e. increasing or decreasing nonlinear SE values. At this stage, modifying linear loading at ports is recommended with first priority because no full-wave simulation is required.

Once the linear analysis is finished, a nonlinear diode grid is to be simulated and the transition between steady-states is to be examined. If more than two steady-states are involved, it is best to investigate each transition part subsequently. For instance, to obtain an intensity band-pass nonlinear SE, two transitions, including intensity dependencies of low-pass and high-pass, have to be investigated individually. If a two-step transition is expected, the grid has to be first simulated by turning all diodes ON and OFF, respectively. Then the diodes at different ports are turned to be either OC or SC according to

a specified gird pattern. If all changes of linear and nonlinear loading at port fail, the structure has to be modified and linear analysis with full-wave simulation is evoked. The optimization is to be iteratively pursued until a satisfying design is found.

In such a manner, four classified manipulations, i.e. shifting, scaling, flipping and combining, can be performed individually at different stages of design, which covers the main requirements of nonlinear SE implementations and saves the optimization cost of simulation. The nonlinear shielding performance of a diode grid can be further modified by changing the relative location of victims inside the enclosure, adding assisted DC biasing to diodes at ports, or even adjusting the distance between diodes in grids.

V. Conclusion

The paper presented a systematic study of nonlinear shielding for an enclosure-backed aperture realized by a diode grid. A hybrid field circuit simulation approach was adopted for numerical analysis and was shown to be efficient for a parameter study of a diode grid. Based on a comprehensive understanding of nonlinear shielding effects both in time and frequency domain, the field intensity selective function of a diode grid was explained and successfully extended from an intensity low-pass type to high-pass, band-stop, band-pass and more types with numerical verification. The OC and SC limits of a diode grid can be effectively adjusted in a dynamic range up to 26 dB. As a result, this work extends the degrees of freedom for designing diode grids, exploits new possibilities of nonlinear field transmissions and shows possibilities of nonlinear shielding application in the future. In the next step, the nonlinear shielding dependence on polarization, bandwidth, position and nonlinear elements, including tunnel diodes, electric discharge (ESD) diodes and transistors, will be investigated.

Acknowledgment

The authors would like to thank Dr.-Ing. Heinz-D. Brüns and Dipl.-Ing. (FH) Angela Freiberg, Hamburg University of Technology (TUHH), Germany, for their support in numerical simulations.

References

[1] W. A. Radasky, C. E. Baum, and M. W. Wik, "Introduction to the special issue on high-power electromagnetics (HPEM) and intentional electromagnetic interference (IEMI)," *IEEE Trans. Electromagn. Compat.*, vol. 46, no. 3, pp. 314–321, 2004.

[2] S. Monni, D. Bekers, M. van Wanum, R. van Dijk, A. Neto, G. Gerini, and F. van Vliet, "Limiting frequency selectice surfaces," in *Proc. 39th Eur. Microw. Conf*, 2009, pp. 606–609.

[3] C. Zhao, C.-F. Wang, and S. Aditya, "Power-dependent frequency-selective surface: Concept, design, and experiment," *IEEE Trans. Antennas Propag.*, vol. 67, no. 5, pp. 3215–3220, 2019.

[4] C. Yang, P. Liu, and X. Huang, "A novel method of energy selective surface for adaptive HPM/EMP protection," *IEEE Antennas Wirel. Propag. Lett.*, vol. 12, pp. 112–115, 2013.

[5] N. Hu, K. Wang, J. Zhang, S. Zha, Z. Wu, C. Liu, and P. Liu, "Design of ultrawideband energy-selective surface for high-power microwave protection," *IEEE Antennas and Wireless Propagation Letters*, vol. 18, no. 4, pp. 669–673, 2019.

[6] J. Zhang, M. Lin, Z. Wu, L. Ding, P. Liu *et al.*, "Energy selective surface with power-dependent transmission coefficient for high-power microwave protection in waveguide," *IEEE Trans. Antennas Propag.*, vol. 67, no. 4, pp. 2494–2502, 2019.

[7] H. Wakatsuchi, S. Kim, J. J. Rushton, and D. F. Sievenpiper, "Waveform-dependent absorbing metasurfaces," *Physical review letters*, vol. 111, no. 24, p. 245501, 2013.

[8] H. Wakatsuchi, J. Long, and D. F. Sievenpiper, "Waveform selective surfaces," *Advanced Functional Materials*, vol. 29, no. 11, p. 1806386, 2019.

[9] S. Vellucci, A. Monti, M. Barbuto, A. Toscano, and F. Bilotti, "Waveform-selective mantle cloaks for intelligent antennas," *IEEE Trans. Antennas Propag.*, vol. 68, no. 3, pp. 1717–1725, 2019.

[10] Z. Luo, X. Chen, J. Long, R. Quarfoth, and D. Sievenpiper, "Nonlinear power-dependent impedance surface," *IEEE Trans. Antennas Propag.*, vol. 63, no. 4, pp. 1736–1745, 2015.

[11] A. Li, S. Kim, Y. Luo, Y. Li, J. Long, and D. F. Sievenpiper, "High-power transistor-based tunable and switchable metasurface absorber," *IEEE Transactions on Microwave Theory and Techniques*, vol. 65, no. 8, pp. 2810–2818, 2017.

[12] Z. Luo, M. Z. Chen, Z. X. Wang, L. Zhou, Y. B. Li, Q. Cheng, H. F. Ma, and T. J. Cui, "Digital nonlinear metasurface with customizable nonreciprocity," *Advanced Functional Materials*, vol. 29, no. 49, p. 1906635, 2019.

[13] M. Kiani, M. Tayarani, A. Momeni, H. Rajabalipanah, and A. Abdolali, "Self-biased tri-state power-multiplexed digital metasurface operating at microwave frequencies," *Optics Express*, vol. 28, no. 4, pp. 5410–5422, 2020.

[14] A. R. Katko, A. M. Hawkes, J. P. Barrett, and S. A. Cummer, "RF limiter metamaterial using pin diodes," *IEEE Antennas and Wireless Propagation Letters*, vol. 10, pp. 1571–1574, 2011.

[15] S. Kim, H. Wakatsuchi, J. J. Rushton, and D. F. Sievenpiper, "Switchable nonlinear metasurfaces for absorbing high power surface waves," *Applied Physics Letters*, vol. 108, no. 4, p. 041903, 2016.

[16] A. Forouzmand, C. S. Kaipa, and A. B. Yakovlev, "Mushroom-type structures with the wires connected through diodes: Theory and applications," *Journal of Applied Physics*, vol. 120, no. 1, p. 015303, 2016.

[17] A. Monti, M. Barbuto, A. Toscano, and F. Bilotti, "Nonlinear mantle cloaking devices for power-dependent antenna arrays," *IEEE Antennas and Wireless Propagation Letters*, vol. 16, pp. 1727–1730, 2017.

[18] Z. Chen, X. Chen, and G. Xu, "A spatial power limiter using a nonlinear frequency selective surface," *International Journal of RF and Microwave Computer-Aided Engineering*, vol. 28, no. 4, p. e21205, 2018.

[19] R. Phon and S. Lim, "Dynamically self-reconfigurable multifunctional all-passive metasurface," *ACS Applied Materials & Interfaces*, vol. 12, no. 37, pp. 42 393–42 402, 2020.

[20] J. Yuan, X. Kong, K. Chen, X. Shen, Q. Wang, and C. Wu, "Intelligent radome design with multilayer composites to realize asymmetric transmission of electromagnetic waves and energy isolation," *IEEE Antennas and Wireless Propagation Letters*, vol. 19, no. 9, pp. 1511–1515, 2020.

[21] M. Barbuto, D. Lione, A. Monti, S. Vellucci, F. Bilotti, and A. Toscano, "Waveguide components and aperture antennas with frequency-and time-domain selectivity properties," *IEEE Transactions on Antennas and Propagation*, 2020.

[22] S. Monni, D. Bekers, M. van Wanum, R. van Dijk, A. Neto, G. Gerini, and F. E. van Vliet, "Protection of rf electronics using tuneable frequency selective surfaces," in *2009 3rd European Conference on Antennas and Propagation*. IEEE, 2009, pp. 3170–3174.

[23] A. R. Katko, A. M. Hawkes, J. P. Barrett, and S. a. Cummer, "RF limiter metamaterial using p-i-n diodes," *IEEE Antennas Wirel. Propag. Lett.*, vol. 10, pp. 1571–1574, 2011.

[24] W. S. Wall, S. M. Rudolph, S. K. Hong, and K. L. Morgan, "Broadband switching nonlinear metamaterial," *IEEE Antennas and Wireless Propagation Letters*, vol. 13, pp. 427–430, 2014.

[25] Y. Loo, H. Wang, H. Zhang, and C. Ong, "Miniaturized power limiter metasurface based on fano-type resonance and babinet principle," *Optics Express*, vol. 24, no. 18, pp. 20 816–20 824, 2016.

[26] D. Qin, R. Ma, J. Su, X. Chen, R. Yang, and W. Zhang, "Ultra-wideband strong field protection device based on metasurface," *IEEE Transactions on Electromagnetic Compatibility*, 2020.

[27] B. Deng, M. Lin, J. Zhang, Z. Wu, C. Liu, and P. Liu, "Pin-diode-based high-intensity radiation fields (hirf) protection of a printed dipole antenna," *IEEE Trans. Electromagn. Compat.*, 2020.

[28] T. Wendt, C. Yang, H. D. Brüns, S. Grivet-Talocia, and C. Schuster, "A macromodeling-based hybrid method for the computation of transient electromagnetic fields scattered by nonlinearly loaded metal structures," *IEEE Trans. Electromagn. Compat.*, vol. 62, no. 4, pp. 1098–1110, 2020.

[29] C. M. Butler, Y. Rahmat-Samii, and R. Mittra, "Electromagnetic penetration through apertures in conducting surfaces," *IEEE transactions on electromagnetic compatibility*, no. 1, pp. 82–93, 1978.
[30] H. A. Mendez, "Shielding theory of enclosures with apertures," *IEEE Transactions on Electromagnetic Compatibility*, no. 2, pp. 296–305, 1978.
[31] M. P. Robinson, T. M. Benson, C. Christopoulos, J. F. Dawson, M. Ganley, A. Marvin, S. Porter, and D. W. Thomas, "Analytical formulation for the shielding effectiveness of enclosures with apertures," *IEEE Trans. Electromagn. Compat.*, vol. 40, no. 3, pp. 240–248, 1998.
[32] P. Dehkhoda, A. Tavakoli, and R. Moini, "An efficient and reliable shielding effectiveness evaluation of a rectangular enclosure with numerous apertures," *IEEE Trans. Electromagn. Compat.*, vol. 50, no. 1, pp. 208–212, 2008.
[33] F. Tesche and T. Liu, "Transient response of antennas with nonlinear loads," *Electron. Lett.*, vol. 11, no. 1, pp. 18–19, 1975.
[34] A. Djordjevic and T. Sarkar, "Transient analysis of electromagnetic systems with multiple lumped nonlinear loads," *IEEE Trans. Antennas Propag.*, vol. 33, no. 5, pp. 533–539, May 1985.
[35] K. Deiseroth and H. Singer, "Transient analysis of nonlinearly loaded arrangements consisting of thin wires and metallic patches," in *Proc. Int. Symp. Electromagn. Compat.* IEEE, 1995, pp. 636–641.
[36] D. Liao, "A hybrid approach for characterizing linear and nonlinear electromagnetic scattering: Theory and applications," Army Research Laboratory, Adelphi, U.S., Tech. Rep. ARL-TR-6261, Nov. 2012.
[37] C. Yang, H.-D. Brüns, P. Liu, and C. Schuster, "Impulse response optimization of band-limited frequency data for hybrid field-circuit simulation of large-scale energy-selective diode grids," *IEEE Trans. Electromagn. Compat.*, vol. PP, no. 99, pp. 1–9, May 2016.
[38] V. A. Thomas, M. E. Jones, M. Piket-May, A. Taflove, E. Harrigan *et al.*, "The use of SPICE lumped circuits as sub-grid models for FDTD analysis," *IEEE microwave and guided wave letters*, vol. 4, no. 5, pp. 141–143, 1994.
[39] A. E. Yilmaz, J.-M. Jin, and E. Michielssen, "A TDIE-based asynchronous electromagnetic-circuit simulator," *Microwave and Wireless Components Letters, IEEE*, vol. 16, no. 3, pp. 122–124, 2006.
[40] R. Wang and J. M. Jin, "Incorporation of multiport lumped networks into the hybrid time-domain finite-element analysis," *IEEE Trans. Microw. Theory Tech.*, vol. 57, no. 8, pp. 2030–2037, 2009.
[41] T. Wendt, C. Yang, C. Schuster, and S. Grivet-Talocia, "Numerical complexity study of solving hybrid multiport field-circuit problems for diode grids," in *2019 International Conference on Electromagnetics in Advanced Applications (ICEAA)*. IEEE, 2019, pp. 90–93.
[42] Matlab2019a. The MathWorks, Natick, MA, USA. [Online]. Available: http://www.mathworks.com/
[43] CONCEPT–II. Institut für Theoretische Elektrotechnik. Hamburg, Germany. [Online]. Available: http://www.tet.tuhh.de/concept/
[44] Pathwave Advanced Design System. Keysight Technologies. California, USA. [Online]. Available: http://www.keysight.com/
[45] B. Gustavsen and A. Semlyen, "Rational approximation of frequency domain responses by vector fitting," *IEEE Trans. Power Deliv.*, vol. 14, no. 3, pp. 1052–1061, 1999.
[46] A. Chinea, S. Grivet-Talocia, S. B. Olivadese, and L. Gobbato, "High-performance passive macromodeling algorithms for parallel computing platforms," *IEEE Trans. Components, Packag. Manuf. Technol.*, vol. 3, no. 7, pp. 1188–1203, Jul. 2013.
[47] CST STUDIO SUITE. Dassault Systèmes. Vélizy-Villacoublay, France. [Online]. Available: http://www.3ds.com/
[48] "Comparison between Si, Ge and GaAs diodes," ConceptsElectronics, Dec. 2014. [Online]. Available: http://conceptselectronics.com/diodes/comparison-si-ge-gaas-diodes
[49] "Varactor SPICE models for RF VCO applications," Application Notes, Skyworks, Aug. 2015. [Online]. Available: https://www.skyworksinc.com/-/media/SkyWorks/Documents/Products/1-100/Varactor_SPICE_Model_AN_200315C.pdf
[50] T. J. Cui, M. Q. Qi, X. Wan, J. Zhao, and Q. Cheng, "Coding metamaterials, digital metamaterials and programmable metamaterials," *Light: Science & Applications*, vol. 3, no. 10, pp. e218–e218, 2014.
[51] T. Konefal, J. F. Dawson, A. C. Marvin, M. P. Robinson, and S. J. Porter, "A fast multiple mode intermediate level circuit model for the prediction of shielding effectiveness of a rectangular box containing a rectangular aperture," *IEEE Trans. Electromagn. Compat.*, vol. 47, no. 4, pp. 678–691, 2005.
[52] M.-C. Yin and P.-A. Du, "An improved circuit model for the prediction of the shielding effectiveness and resonances of an enclosure with apertures," *IEEE Trans. Electromagn. Compat.*, vol. 58, no. 2, pp. 448–456, 2016.
[53] J. Shim, D. G. Kam, J. H. Kwon, and J. Kim, "Circuital modeling and measurement of shielding effectiveness against oblique incident plane wave on apertures in multiple sides of rectangular enclosure," *IEEE Trans. Electromagn. Compat.*, vol. 52, no. 3, pp. 566–577, 2010.

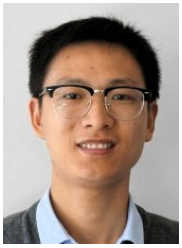

Cheng Yang (M'17) received his B.S. degree in electronic science and technology from Wuhan University (WHU), Wuhan, China, in 2009, the M.S. degree and the Ph.D. Degree with electromagnetic field and microwave technology from the National University of Defense Technology (NUDT), Changsha, China, in 2012 and 2016.

Since 2019 he has been a senior engineer of the Institute of Electromagnetic Theory, Technische Universität Hamburg (TUHH), Hamburg, Germany. From 2013 to 2015, he was funded by the Chinese Scholarship Council (CSC) as a joint-PhD student at TUHH. From 2017 to 2019, he was a Faculty Member of the State Key Laboratory of Millimeter Wave at Southeast University (SEU), Nanjing, China. His current research interests include computational electromagnetics, microwave measurement techniques, electromagnetic compatibility and biology electromagnetics.

Torben Wendt (S'17) received his B.S. and M.S. degree in electrical engineering from the Technical University Hamburg (TUHH), Hamburg, Germany, in 2014 and 2017, respectively.

Currently, he is working towards the Ph.D. degree at the Institute of Electromagnetic Theory, TUHH. He was a visiting researcher at the Politecnico di Torino for multiple times in 2018 and 2019. His current research interests include the modeling and simulation of nonlinear field circuit coupling in EMC applications.

Marco De Stefano received the M.Sc. degree in mechatronic engineering from Politecnico di Torino, Turin, Italy, in 2018, where he is currently pursuing the Ph.D. degree in electrical, electronics and communication engineering. His research interests include model-order reduction, with emphasis on parameterized macromodeling, and fast simulation methods for signal and power integrity.

Mr. De Stefano was a co-recipient of the 2018 Best Paper Award of the IEEE INTERNATIONAL SYMPOSIUM ON ELECTROMAGNETIC COMPATIBILITY and the 2019 Best Student Paper of the IEEE WORKSHOP ON SIGNAL AND POWER INTEGRITY.

Marc Kopf received the B.Sc. and M.Sc. degrees in electrical engineering, respectively 2017 and 2020 from Hamburg University of Technology (TUHH), Hamburg, Germany.

After a trip into the world of startups, he will start to pursue a Ph.D. in electrical engineering as Marie Skłodowska-Curie Early Stage Researcher with the Eindhoven University of Technology (TU/e), Eindhoven, The Netherlands by July 2021. His research will focus on developing a generic approach to quantify the EMI-impact of medical devices on their environment as part of the European Training Network on Electromagnetic Risks in Medical Technology (ETERNITY).

Christopher Marc Becker received his B.S. degree in computer science engineering from Technische Universität Hamburg (TUHH), Hamburg, Germany, in 2019. Since 2019 he is studying Computer Science M.Sc. and expects to receive his degree in spring 2022. His latest work regarding his current thesis is concurred with Machine Learning on the topic federated learning. Besides his study, he works as an IT-Manager/Programmer in a Start-Up based in Hamburg since 2019.

Stefano Grivet-Talocia (M'98–SM'07–F'18) received the Laurea and Ph.D. degrees in electronic engineering from the Politecnico di Torino, Turin, Italy.

From 1994 to 1996, he was with the NASA/Goddard Space Flight Center, Greenbelt, MD, USA. He is currently a Full Professor of electrical engineering with the Politecnico di Torino. He co-founded the academic spinoff company IdemWorks in 2007, serving as the President until its acquisition by CST in 2016. He has authored over 180 journal and conference papers. His current research interests include passive macromodeling of lumped and distributed interconnect structures, model-order reduction, modeling and simulation of fields, circuits, and their interaction, wavelets, time-frequency transforms, and their applications.

Dr. Grivet-Talocia was a co-recipient of the 2007 Best Paper Award of the IEEE TRANSACTIONS ON ADVANCED PACKAGING. He received the IBM Shared University Research Award in 2007, 2008, and 2009. He was an Associate Editor of the IEEE TRANSACTIONS ON ELECTROMAGNETIC COMPATIBILITY from 1999 to 2001 and He is currently serving as Associate Editor for the IEEE TRANSACTIONS ON COMPONENTS, PACKAGING AND MANUFACTURING TECHNOLOGY. He was the General Chair of the 20th and 21st IEEE Workshops on Signal and Power Integrity (SPI2016 and SPI2017).

Christian Schuster (S'98 - M'00 - SM'05) received the Diploma degree in physics from the University of Konstanz, Germany, in 1996, and the Ph. D. degree in electrical engineering from the Swiss Federal Institute of Technology (ETH), Zurich, Switzerland, in 2000. Since 2006 he is full professor and head of the Institute of Electromagnetic Theory at the Hamburg University of Technology (TUHH), Germany. Prior to that he was with the IBM T. J. Watson Research Center, Yorktown Heights, NY, where he was involved in high-speed optoelectronic package and backplane interconnect modeling and signal integrity design for new server generations. His currents interests include signal and power integrity of digital systems, multiport measurement and calibration techniques, and development of electromagnetic simulation methods for communication electronics.

Dr. Schuster received IEEE Transactions on EMC Best Paper Awards in 2001 and 2015, IEEE Transactions on CPMT Best Paper Awards in 2012 and 2016, IEC DesignCon Paper Awards in 2005, 2006, 2010, 2017 and 2018, three IBM Research Division Awards between 2003 and 2005, and IBM Faculty Awards in 2009 and 2010. Also, in 2019 he received the Sustained Service to the EMC Society Award. He is a member of the German Physical Society (DPG) and several technical program committees of international conferences on signal and power integrity, and electromagnetic compatibility. He was serving as a Distinguished Lecturer for the IEEE EMC Society in the period 2012-2013, as the Chair of the German IEEE EMC Chapter in the period 2016-2019 and is currently an Associate Editor for the IEEE Transactions on EMC, a member of the Board of Directors of the EMC Society, and an Adjunct Associate Professor at the School of Electrical and Computer Engineering of the Georgia Institute of Technology.